Received: 14 January 2022 | Revised: 13 June 2022 | Accepted: 2 July 2022

DOI: 10.1002/eqe.3714

RESEARCH ARTICLE

WILEY

A macro-model for describing the in-plane seismic response of masonry-infilled frames with sliding/flexible joints

Prateek Kumar Dhir[1] | **Enrico Tubaldi**[1] | **Bartolomeo Pantò**[2] | **Ivo Caliò**[3]

[1]Department of Civil and Environmental Engineering, University of Strathclyde, Glasgow, UK

[2]Department of Engineering, Durham University, Durham, UK

[3]Department of Civil Engineering and Architecture, University of Catania, Catania, Italy

Correspondence
Prateek Kumar Dhir, Department of Civil and Environmental Engineering, University of Strathclyde, Glasgow G1 1XJ, UK.
Email: prateek.dhir@strath.ac.uk

Abstract

Masonry infill walls are among the most vulnerable components of reinforced concrete (RC) frame structures. Recently, some techniques for enhancing the performance of the infills have been proposed, aiming at improving both the global and the local behaviour of the infilled frame structure. Among the most promising ones, there are those that aim to decouple or reduce the infill-frame interaction by means of flexible or sliding joints, relying respectively on rubber or low-friction materials at the interface between horizontal subpanels or between the panels and the frame. Numerous models have been developed in the last decades for describing the seismic response of masonry-infilled RC frames, but these have focused mainly on the case of traditional infills. This study aims to fill this gap by proposing a two-dimensional macro-element model for describing the in-plane behaviour of RC infilled frames with flexible or sliding joints. The proposed modelling approach, implemented in OpenSees, is an extension of a discrete macro-element previously developed for the case of traditional infill panels. It is calibrated and validated in this study against quasi-static tests from the literature, carried out on masonry-infilled RC frames with sliding and rubber joints. The study results show the capabilities of the proposed modelling approach to evaluate the benefits of using flexible joints in terms of minimising the negative effects of the interaction between infill and RC frame and limiting the increase of global stiffness of the system with respect to the bare frame condition.

KEYWORDS

macro-element, masonry infills, non-structural components, rubber joints, sliding joints

1 | INTRODUCTION

Masonry infills are among the most vulnerable components of reinforced concrete (RC) building frames. They are often disregarded in the design stage, and because of this, they often undergo severe cracking and damage even under moderate earthquakes. Their collapse can cause injuries, life losses, and delays in rescue operations and post-earthquake recovery.

Many studies (e.g.,[1,2]) have highlighted the considerable economic losses associated with infill walls' damage, and have shown that the repair cost of these can be significantly higher than that of structural components.

The improvement of the seismic performance of infill walls and RC infilled frames has been a subject of considerable research in the last decades, with many technical solutions proposed and experimentally tested. Some solutions aim at increasing the resistance of the infill.[3,4] However, these techniques are often not cost effective and require the strengthening of the frame members, due to the transmission of increased forces to them from the infills. Alternative solutions have been proposed that aim to increase the flexibility of the infill panel and/or to reduce its interaction with the surrounding frame, through the introduction of sliding joints[5–11] or flexible/soft layers[12–18] within the panel or between the panel and the surrounding frame. The use of joints, where most of the deformations are localised, allows reducing the stresses, and thus the damage, in the infill panel as well as minimising the interaction between the panel and the surrounding frame. Another benefit brought by the joints is that they permit to control the increase of global stiffness of the infilled frame, which can significantly alter the seismic demand with respect to the bare frame condition. The joints can also contribute to the energy dissipation, reducing the seismic demand on structural and non-structural components.

The numerical simulation of the seismic performance of infilled frames is a computationally challenging task due to the nonlinearity of the materials involved, the complex interaction between the infills and the main frame structure, and the various possible failure modes that could occur. Different modelling approaches have been proposed, including macro modelling and micro/meso-scale modelling[19–21] (see e.g.,[22] for a review of the state of the art). Some of these approaches have also been applied to model infilled frames with flexible/sliding joints.[7–9,12–15,17,18]

Detailed numerical analyses involving micro and meso-scale descriptions of masonry can be computationally costly and unsuitable for large scale structures. In this case, macro-models are found to be very appealing due to the reduced number of degrees of freedom and parameters that are required to define them. Many of the simplified models for masonry infilled frames rely on the concept of equivalent strut.[23–25] A two-dimensional (2D) discrete macro-element (DMEM) model for infill frames was proposed by Caliò and Pantò[19] to avoid the main limitations of the equivalent strut approach. This macro-model, originally proposed for unreinforced masonry buildings[26] has been implemented in the software 3DMacro[27] and validated against experimental tests by Marques and Lourenço.[28] More recently, Pantò and Rossi[29] implemented a simplified version of the DMEM model, already proposed in,[19] but characterised by a limited number of nonlinear links along the interfaces between elements in order to allow its implementation in the FE program OpenSees.[30]

In the context of simplified modelling of RC infill frames with sliding joints, Preti et al.[7] developed an analytical formulation for calibrating the properties of an equivalent strut based on the geometrical and mechanical properties of the infill panel and of the sliding joints. This model was used by Di Trapani et al.[9] to assess the benefits of using sliding joints in improving the seismic performance of masonry-infilled RC frames. To date, no study has investigated the use of 2D macro-models for investigating the behaviour of RC frames with sliding/flexible joints under in-plane loading.

The present study aims to fill this gap by extending the 2D macro modelling strategy, originally developed by Caliò and Pantò,[19] for RC frames with traditional infills to the case of infills with flexible/sliding joints. Section 2 of the manuscript illustrates the proposed modelling strategy, involving the 2D macro-element implemented in Opensees,[29] and Section 3 describes the outcomes of the numerical calibration study carried out by considering numerous experimental tests[10,31,32] and advanced numerical analyses[8,33] performed on RC frames infilled with sliding/flexible joints. The results of the proposed model are validated against experimental tests and other numerical approaches present in the literature.

2 | THE PROPOSED MODELLING STRATEGY

This section illustrates the modelling strategy developed for describing the hysteretic behaviour of a masonry-infilled frame with flexible/sliding joints that are horizontally placed between the infill sub-panels and vertically at the column-infill interfaces (see Figure 1). The same modelling strategy can also be used to describe alternative configurations[11] not explicitly addressed in this paper.

The proposed modelling approach is based on the discrete macro-element method (DMEM) originally developed by Caliò and Pantò,[19] subsequently implemented in a simplified version in OpenSees by Pantò and Rossi.[29] The proposed model can be represented by an equivalent mechanical scheme consisting in an articulated quadrilateral (Figure 2A). Two uni-directional diagonal links and eight bi-directional perimetral contact links describe the shear and flexural behaviour of the represented masonry portion of masonry, respectively. The latter 2D links, also describe the normal and tangential behaviour of the infill-frame interfaces. Following the simplified formulation developed in,[29] the two 2D links placed on each rigid edge of the panel allow the macro-element to interact with adjacent macro-elements or to frame beam/column

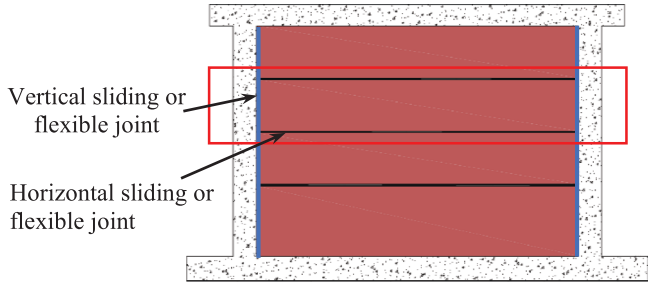

FIGURE 1 Reinforced concrete infill frame equipped with horizontal and vertical sliding/flexible joints

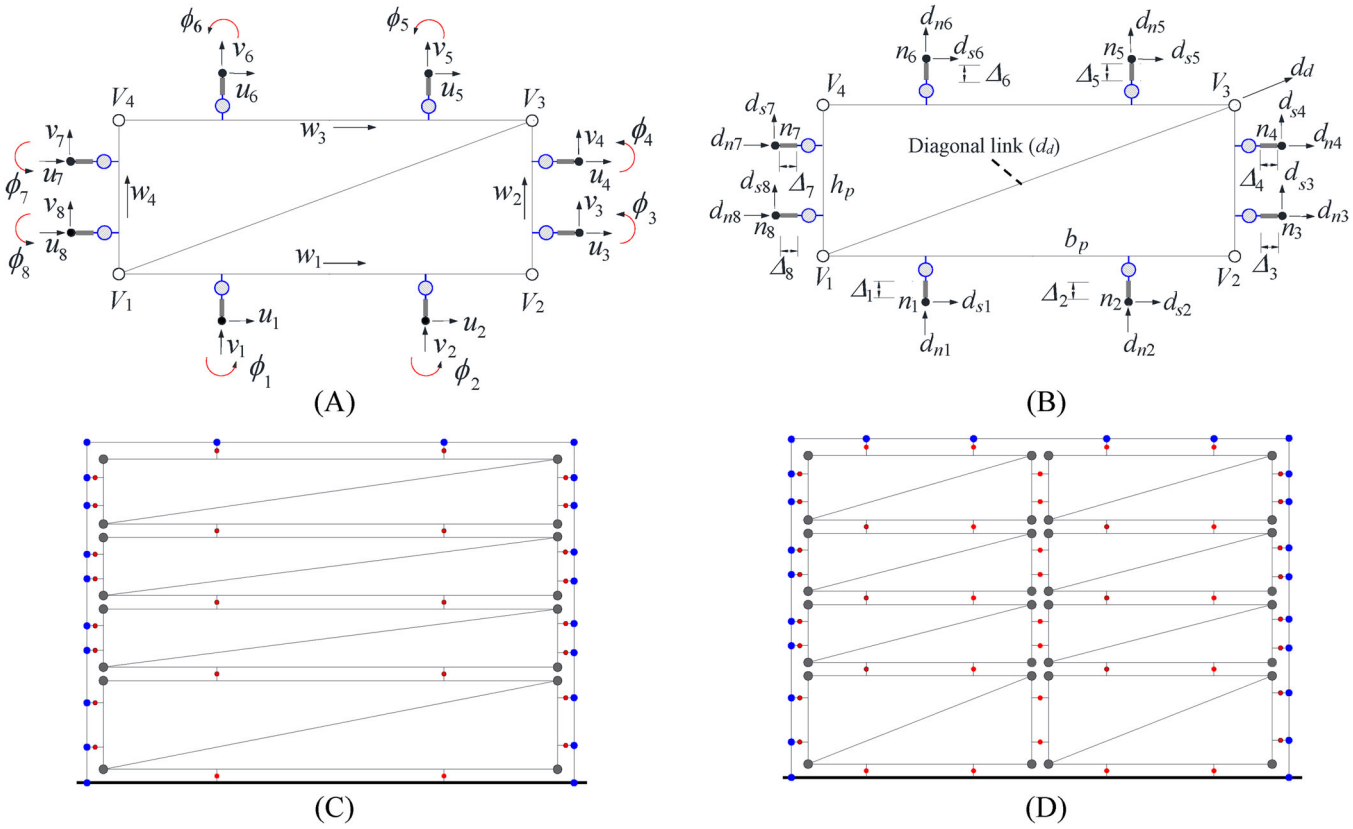

FIGURE 2 (A) Degrees of freedom of the macro-element, (B) generalised deformations, (C) discretisation of the infill with joints into minimum number of subpanels, (D) more refined discretisation

elements. The deformability of the 2D links is concentrated in two zero-length nonlinear coupled springs connected in-series with rigid offsets (Δ_i), with $i = 1\ldots8$, shown in Figure 2A. Each link is located at one-fourth of the panel edge length (b_p or h_p) from the vertexes (V_i) (i = 1… 4), which allow for a geometrically consistent description of the interaction between infills and beam or column elements.[29] Each macro-element possesses eight nodes (n_i), *with* $i = 1\ldots8$, connecting the macro-element with the adjacent macro-elements and frame elements (Figure 2A). Each macro-element is kinematically characterised by 28 degrees of freedom (Figure 2A), 24 of which are associated with the translations and rotations of nodes (u_i, v_i, ϕ_i) with $i = 1\ldots8$, and four (w_i … w_4) describing the rigid motion and shear-deformation of the panel. These dofs can be kinematically related to 17 generalised deformations: 16 deformations related to the normal ($d_{n1}\ldots d_{n8}$) and tangential ($d_{s1}\ldots d_{s8}$) deformations of the 2D links and the deformation of the internal diagonal link (d_d), shown in Figure 2B.

In the case of traditional infills, the response of the contact links along the normal direction describes the flexural response of the represented portion of the infill. The link shear response describes the sliding between the infill or between the infills and the surrounding frame members. The diagonal link describes the diagonal shear failure of the infill. It is assumed that the uniaxial response of the diagonal link depends only on the shear deformation of the articulated quadrilateral and does not vary with the change in axial forces along the horizontal and vertical direction. It is noteworthy that in reality the infill is usually built after the surrounding frame, and thus it contributes to withstanding the permanent loads other than dead-weight, and the variable loads acting in the frame. Moreover, the compressive forces in the infills are also expected to change during the earthquake motion.[20] However, the simplified hypothesis of considering the infill shear response independent to the confinement has been accepted in the literature and validated against experimental tests.[29,34]

In the case of infills with sliding/flexible joints, the macro-element link properties depend on the type of discretisation adopted. For example, in Figure 2C the number of macro-elements is equal to the number of subpanels identified by the horizontal joints (Figure 1). Thus, each macro-element describes a masonry subpanel surrounded by flexible/sliding joints. The normal component of the 2D contact links describes the tensile/compressive behaviour of the masonry subpanels and of the sliding/flexible joints, working as a series mechanical system, whereas the tangential component of the 2D contact links describes the sliding of the low-friction joints or the shear displacement of the sliding/flexible joints. The diagonal link simulates the diagonal shear behaviour of the masonry subpanels and its properties are not affected by the sliding/flexible joints. The next subsections describe the calibration of the macro-element properties for this type of discretisation. It is noteworthy that each subpanel could be discretised into more than one macro-element (Figure 2D). The properties of the links for the macro-elements used in Figure 2D can be found by combining the modelling strategy described in the following subsections with the ones already developed in[29] for the case of traditional masonry infills. According to the original formulation proposed by Caliò and Pantò,[19] a single macro-element could be employed for describing the entire infill-joint system. However, in presence of sliding/flexible joints, it is necessary to consider a mesh of macro-elements, consistent with the distribution of the joints, in order to describe the interaction between adjacent horizontal subpanels and between the subpanels and the surrounding frame.

The simplified hypothesis of connecting each panel edge by two links may introduce an approximation in describing the local behaviour of the infill and its interaction with the frame members. However, as evidenced in Pantò and Rossi[29] and confirmed by the results presented in this study, the proposed model can describe the global response of infilled frames with a reasonable level of accuracy, even employing a coarse mesh of macro-elements.

2.1 | The 2D contact link

Figure 3A shows the equivalent mechanical scheme of the 2D nonlinear link. The relative displacements of the link along the normal and tangential direction, collected in the vector $\mathbf{q} = [d_n \; d_s]$, and the dual internal forces, collected in vector $\mathbf{Q} = [F_n \; F_s]$, are related through the expression $\delta\mathbf{Q} = \mathbf{K}\delta\mathbf{q}$ where δ denotes the variation operator, and $\mathbf{K}$ denotes the tangent stiffness matrix of the link, expressed as follows:

$$\mathbf{K} = \begin{pmatrix} K_n & 0 \\ 0 & K_s \end{pmatrix} \tag{1}$$

where K_n and K_s are the tangent stiffnesses of the link in the normal and tangential directions, respectively.

The Concrete02 material model, implemented in OpenSees,[30] is used to describe the normal response of the contact link. The nonlinear elastoplastic model employed in[35] is employed to simulate the masonry response in compression, whereas a bi-linear constitutive law with linear strength degradation simulates the response in tension. These constitutive models efficacy allow for cyclic stiffness degradation with the increase of the normal strain. The essential parameters to describe the normal response envelope of the 2D link Figure 3B, are: the initial elastic stiffness (K_{nm}), the maximum compressive force (F_{cm}), the maximum tensile force (F_{tm}), the ultimate displacement in compression (d_{cm}), the ultimate displacement in tension (d_{tm}) and the residual compressive strength (F_{rm}). The parameter λ represents the ratio between the unloading stiffness and the initial stiffness and controls the cyclic material behaviour.

In general, the values of the parameters of Figure 3B depend on the geometry of the macro-element and on the mechanical properties of the masonry infill and of the flexible/sliding joints, which form a series mechanical system. The properties defining the normal behaviour of the sliding/flexible joints, assuming an elastic-perfectly plastic constitutive law, are the

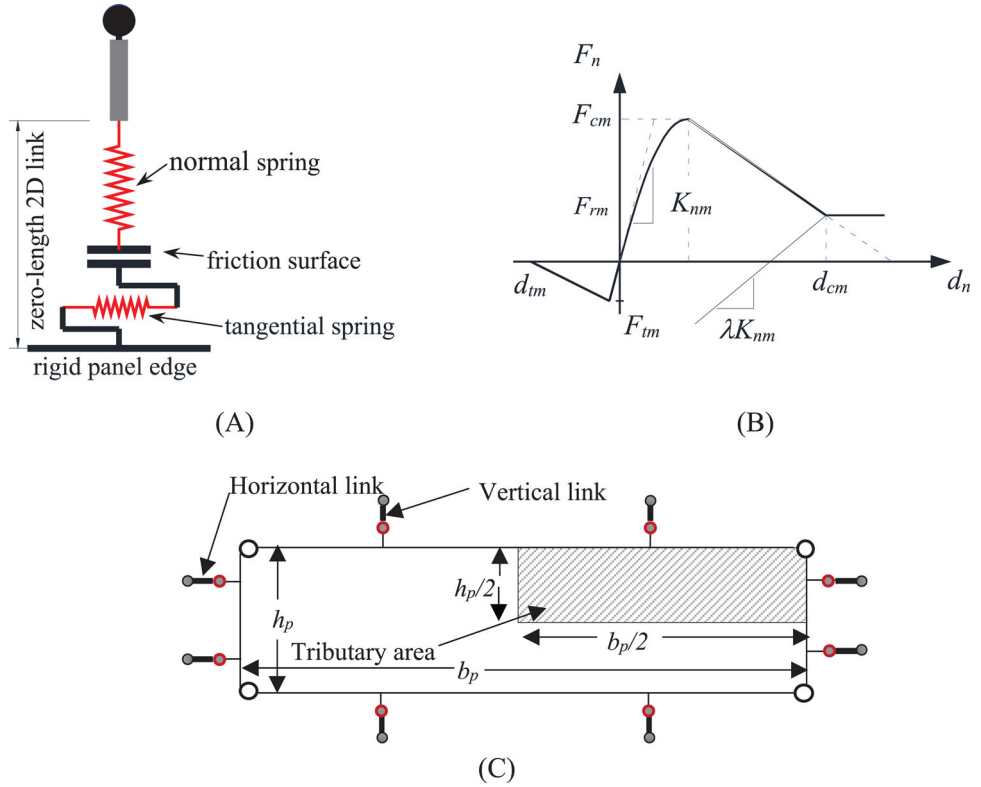

FIGURE 3 (A) Equivalent mechanical scheme of 2D contact link, (B) cyclic response in normal direction, (C) tributary masonry area

TABLE 1 Mechanical parameters of the normal response of the equivalent normal spring representing the masonry panel (after[29])

Initial stiffness	Maximum compressive force	Maximum tensile force	Residual compressive force	Ultimate compression. displacement	Ultimate tensile displacement
$K_{nm} = \frac{E_m A_p}{l_p}$	$F_{cm} = f_{cm} A_p$	$F_{tm} = f_{tm} A_p$	$F_{rm} = f_{rm} A_p$	$d_{cm} = \varepsilon_{cu} l_p$	$d_{tm} = \varepsilon_{tu} l_p$

initial normal stiffness per unit area k_{nj}, the tensile strength f_{tj}, and the compressive strength f_{cj}. The following mechanical parameters are used to characterise the constitutive behaviour of the masonry, considered as a homogenised continuous orthotropic material characterised along each direction of orthotropy by: initial Young's modulus (E_m), compression and tensile strengths (f_{cm},f_{tm}) and the corresponding ultimate strains in tension and compression (ε_{cu}, ε_{tu}) and a residual compressive strength f_{rm}. A tributary panel area (see Figure 3C) is considered for defining the contribution of the masonry subpanel. Let w_p, b_p and h_p denote, respectively, the thickness, width and height of the subpanel contributing to the normal link. In order to define the normal link properties (Figure 2B), the continuous masonry portion of the subpanel is replaced by an equivalent discrete one, whose properties are described in Table 1, where A_p and l_p represent, respectively, the cross-section area and the length of the tributary volume of the subpanel associated with the link. These are equal to respectively $w_p b_p/2$ and $h_p/2$ in the case of the vertical contact link Figure 3B. If flexible/sliding joints are present at the edge of the panel, then their properties must be combined with those of Table 1, using a series mechanical model representation.

In the case of a macro-element representing a subpanel interacting with the frame through a horizontal or vertical sliding/flexible joint, the normal stiffness of the contact link, evaluated combining in series the stiffness representing the masonry panel (K_{nm}), and the normal stiffness of the joint (K_{nj}), is obtained as follows:

$$K_n = \frac{K_{nm} K_{nj}}{K_{nm} + K_{nj}} \tag{2}$$

The stiffness of the joint K_{nj} can be evaluated by multiplying the stiffness per unit area k_{nj} by the tributary area of the joint A_p.

In the case of two macro-elements representing two subpanels separated by a sliding/flexible joint, each panel link is associated to the deformability of masonry and of half joint. Equation (2) becomes:

$$K_n = \frac{2K_{nm}K_{nj}}{K_{nm} + 2K_{nj}} \tag{3}$$

The tensile (compressive) resistance of the series system is equal to the lowest value among the tensile (compressive) resistance of the two components.

The shear response of the contact links of the macro-element is assumed to be controlled by the mechanical behaviour of the joints at the edges of the macro-element. In the case of rubber joints, the shear stiffness of the 2D link K_s coincides with that of the joint K_{sj}, which can be taken equal to the rubber stiffness assuming that the rubber compliance is much higher than that of the mortar joints (see Dhir et al.[36]). The behaviour of rubber in simple shear is very complicated, since it is rate-dependent, amplitude-dependent, and characterised by the Mullins effect.[37] In this study, a linearised behaviour (constant stiffness) is considered for simplicity. In the case of sliding joints, a very high value of K_{sj} can be assumed until sliding takes place. The tangent shear stiffness can be assumed to be zero during sliding.

The shear capacity of the contact links is described by an elasto-plastic model with an associated Mohr-Coulomb yield surface characterised by the following parameters: the cohesion c_j, the friction coefficient μ_j, the tributary contact area of the link A_p. For simplicity, the values of c and μ are assumed to be constant and the unloading/reloading tangential stiffness is assumed equal to the initial elastic one. It is noteworthy that also in the case of rubber joints sliding may occur following bond failure (usually at the rubber joint-mortar interface).

2.2 | The diagonal link

As already discussed above, it is assumed that the minimum number of macro-elements is equal to the number of subpanels identified by the horizontal joints. According to this strategy, the diagonal link represents the shear behaviour of the masonry subpanel, since the deformability of the flexible/sliding joints is described entirely by the 2D contact links along the panel perimeter (Figure 4A). The uniaxial material Pinching4, which is already available in OpenSees,[30] is used to simulate the axial force-displacement (F_d, d_d) response of the diagonal link (Figure 4B).[38,39]

The constitutive law of the diagonal link is assumed not to depend on the compression forces acting on the vertical and horizontal edges of the panel. It only depends on the shear deformation of the articulated quadrilateral. This is a simplification that is not expected to lead to significant errors in the response assessment. The envelope curve describing this response is defined by eight parameters, i.e. F_{1d}, d_{1d}; F_{2d}, d_{2d}; F_{3d}, d_{3d}; F_{4d}, d_{4d}, which are indicated in Figure 4B. These parameters are calibrated according to the macroscopic shear parameters of masonry, which can be identified by performing laboratory tests on masonry panels, and the panel geometry. The calibration procedure consists in imposing an equivalence between the discrete model and an equivalent continuous subpanel subjected to a pure shear stress state.[29] The results are summarised in Table 2. More specifically, the mechanical behaviour of masonry is characterised by the

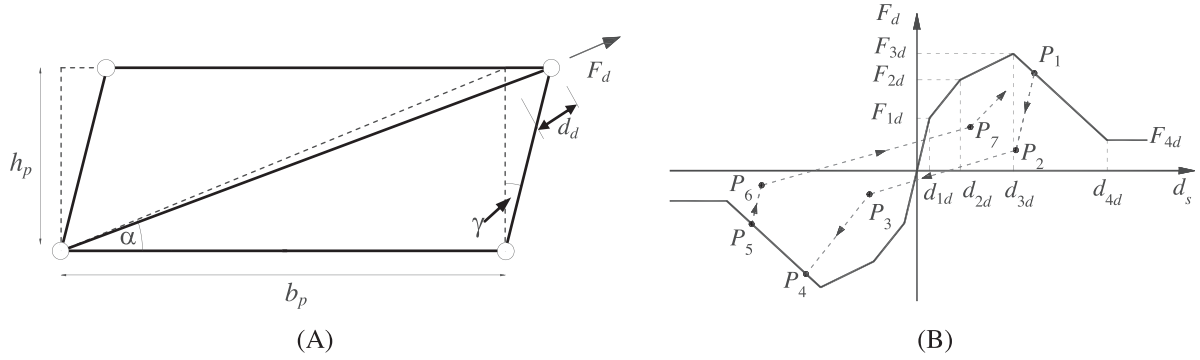

FIGURE 4 (A) Mechanical scheme and (B) cyclic response of the diagonal link

TABLE 2 Mechanical parameters of the response envelope of the diagonal link[29] ($\alpha = \arctan(h_p/b_p)$ is the angle between the diagonal and the first edge of the panel)

Cracking force	Yielding force	Peak force	Residual force	Initial stiffness	Yielding displacement	Peak-force displacement	Residual-force displacement
$F_{1d} = \frac{\tau_{cr} w_p b_p}{\cos\alpha}$	$F_{2d} = \frac{\tau_y w_p b_p}{\cos\alpha}$	$F_{3d} = \frac{\tau_0 w_p b_p}{\cos\alpha}$	$F_{4d} = \frac{\tau_r w_p b_p}{\cos\alpha}$	$K_{d_0} = \frac{G_m w_p b_p}{h_p \cos^2\alpha}$	$d_{2d} = h_p \gamma_y \cos\alpha$	$d_{3d} = h_p \gamma_0 \cos\alpha$	$d_{4d} = h_p \gamma_r \cos\alpha$

initial shear modulus (G_m) and the shear stress corresponding to cracking (τ_{cr}); the stress/drift at the yield (τ_y, γ_y), peak (τ_0, γ_0) and residual (τ_R, γ_R) strengths. Each strength describes a specific macroscopic level of damage. In particular, the *cracking* strength describes the end of the elastic response of the infill, corresponding to the activation of microcracks. In addition, the *yield* strength allows a better description of the change of infill shear stiffness due to the opening of macrocracks.

A cyclic constitutive law with a pinching effect, already implemented in OpenSees[30] and characterised by a trilinear unload-reload path,[29] is adopted. The model takes into account for the degradation of the reloading stiffness and strength by means of two damage indexes, D_k and D_r, whose evolution is described by the following equation:

$$D_h = 1 - \alpha_h [E_{cum} / (\eta_h E_{mon})]^{\beta_h} \leq D_{h,\text{lim}} \qquad h = k, r \tag{4}$$

where the parameters α_h, β_h and η_h, are constitutive parameters of the damage model, $D_{k,\text{ lim}}$ and $D_{r,\text{ lim}}$ the two limit values of damage indexes, E_{cum} the cumulative energy at the current step of the analysis, and E_{mon} is the ultimate cumulative energy corresponding to a monotonic process. The parameters of the cyclic and damage models can be adjusted to obtain the best fit to the experimental results.

3 | NUMERICAL SIMULATIONS

In this section, a validation study is conducted in view of the experimental tests performed by Calvi and Bolognini[31] on a RC frame infilled with traditional hollow bricks under in-plane load (case study I). A further comparison is then performed considering the numerical investigation performed with an advanced 2D finite element (FE) modelling approach by Bolis et al.[8] (case study II) on the same bare frame, with different infill typology and with the addition of sliding joints. Finally, the experimental tests performed within the INSYSME project[32] on an RC frame with traditional masonry infills and masonry infills with mortar-rubber joints under in-plane loading (case study III) are considered to further demonstrate the abilities of the proposed modelling approach.

3.1 | Case study I: Traditional infill (after Calvi and Bolognini[31])

The first case study consists in a masonry-infilled RC frame experimentally tested by Calvi and Bolognini.[31] Figure 5 provides some details of the frame and masonry infill, including the concrete member sizes, diameters of the steel rebars

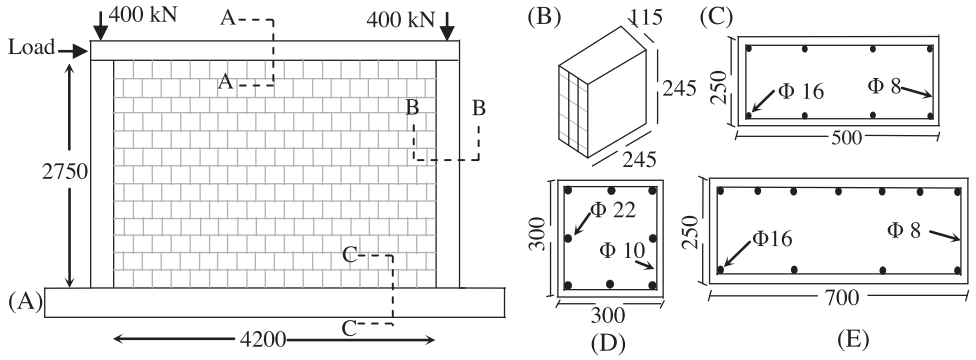

FIGURE 5 Geometric details (dimensions in mm) of (A) the tested infilled frame (B) the perforated clay block units, (C) top beam (section A-A), (D) column (section B-B), and (E) top beam (section C-C)

TABLE 3 Mechanical parameters of concrete and steel reinforcement

Mechanical properties	Concrete	Steel reinforcement	Source
Young's modulus, E (MPa)	22,000	210,000	31
Poisson ratio, v (-)	0.15	0.3	31
Compressive strength, f_c (MPa)	29.32 (column), 34.56 (beam)	–	31
Yield strength (MPa)	–	557	31
Tensile strength f_t (MPa)	3.9	–	31
Post-elastic to elastic stiffness ratio	–	0.002	8

TABLE 4 Mechanical parameters of the masonry for defining the contact normal links

Direction	E_m (MPa)	f_{cm} (MPa)	f_{tm} (MPa)	f_{rm} (MPa)	ε_{cu} (-)	ε_{tu} (-)	λ (-)	Source
Horizontal	991	1.11	0.10	0.20	0.4	0.002	0.1	8,31
Vertical	1873	1.10	0.52	0.22	0.4	0.006	0.1	8,31

TABLE 5 Mechanical parameters of the contact links in shear describing the frame-infill interaction

Parameter	CM	BBM	TBM	Source
k_j (N/mm^3)	150	200	100	Proposed model
c_j (MPa)	0.41	0.41	0.41	8,31
μ_j (-)	0.80	1.00	0.40	8,31

and masonry block dimensions. Perforated clay blocks were selected (typical of European earthquake-prone countries), and laid with holes running horizontally. The bed and head joints are 10 mm thick. Further details regarding the prototype are available in literature.[31] The experimental tests were conducted on the bare frame (BF) and the frame with traditional infills (TIF) subjected to in-plane loading. In the tests, vertical loads (400 kN) were initially applied at the top of the two columns to simulate the effect of permanent loads acting on the frame, followed by an in-plane horizontal load, monotonic or cyclic, applied at the beam's left extremity, as shown in Figure 5. Forced-based non-linear beam elements with two Legendre integration points are used to describe both the beams and columns, with the cross-sections discretised into fibres. The discretisation of the frame elements depends on that of the infill. In particular, since a single macro-element is used for the infill, each frame element of the RC frame is subdivided into three elements to allow the connection of the frame elements to the external nodes of the infill macro-element.

Table 3 reports the main mechanical properties of the concrete and steel reinforcement used for the RC frame members. Table 4 reports the parameters characterising the normal behaviour of masonry panel along the horizontal and vertical direction. Table 5 reports the properties of the frame-infill interfaces, namely column-masonry (CM), bottom beam-masonry (BBM), top beam-masonry (TBM), panel-panel in horizontal direction (PPH) and panel-panel in vertical direction (PPV). Table 6 contains the parameters that define the diagonal link envelope curve. The values of the properties displayed in Table 3-Table 6 are based on the reported material properties of concrete and steel, on the experimental tests on masonry panels carried out by Calvi and Bolognini,[31] and on the parameters adopted by Bolis et al.[8] to simulate these tests. G_{m} comes from the value of E_{m} assuming a poisson ratio of 0.2.[29] The values of some parameters, such as those

TABLE 6 Mechanical parameters of the masonry for defining the response envelope of the diagonal link

G_m, Shear modulus (MPa)	τ_{cr}, Cracking stress (MPa)	τ_y, Yielding stress (MPa)	τ_0, Peak stress (MPa)	τ_r, Residual stress (MPa)	γ_{cr}, Diagonal shear drift (-)	γ_y, Yield shear drift (-)	γ_0, Peak shear drift (-)	γ_r, Residual shear drift (-)	source
418	0.236[a]	0.329[a]	0.364	0.109[a]	0.00057[a]	0.00392[a]	0.00784[a]	0.02510[a]	8,31

[a]This parameter has been evaluated to provide by fitting the experimental results.

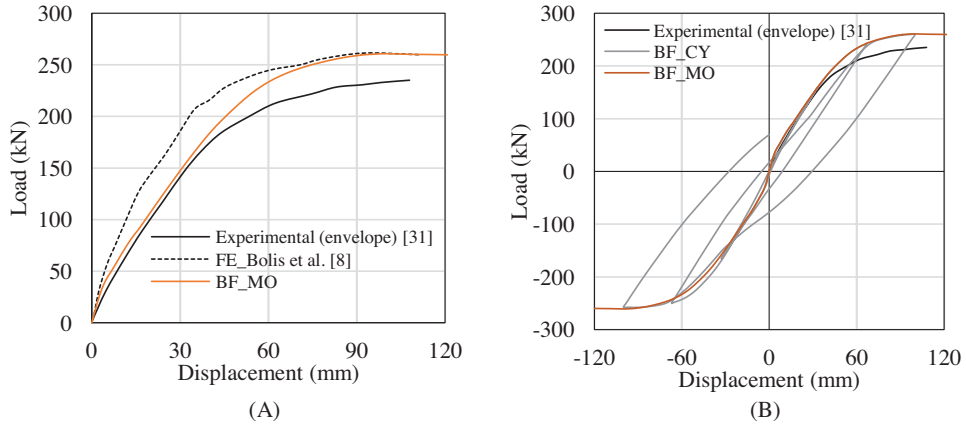

FIGURE 6 Comparison between numerical and experimental load-displacement curves for bare frames against (A) monotonic and (B) cyclic loading

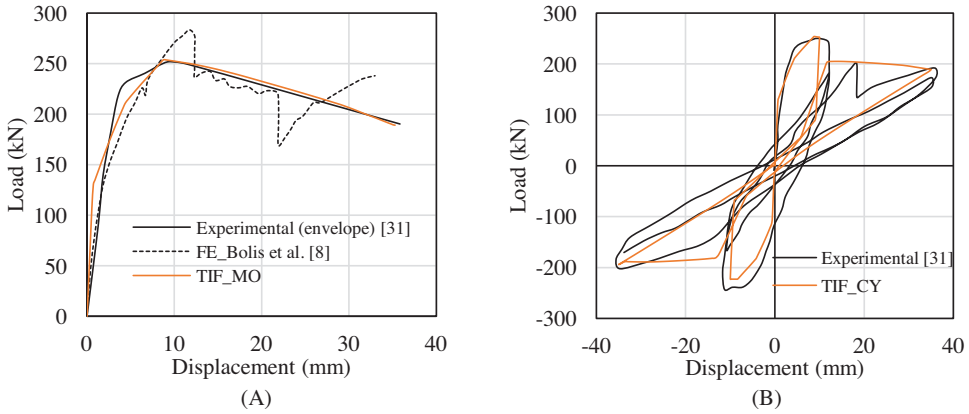

FIGURE 7 Load-displacement curves of infilled frames against (A) monotonic and (B) cyclic loading

TABLE 7 Comparison of elastic stiffness and ultimate load according to experimental tests and numerical predictions

	K_e (N/mm)	Err-K_e (%)	F_{max} (kN)	Err-F_{max} (%)
Experimental (envelope)[31]	14.55	–	251.77	–
FE_Bolis et al.[8]	17.36	16.21	283.53	11.20
Proposed model (TIF_MO)	18.55	21.55	253.91	0.84

defining the cracking and yield point, have been chosen among a range of possible values to provide the best fit to the experimental results.

In Figure 6A, the monotonic force-displacement response of the bare frame obtained by the proposed model (BF_MO) is compared with the experimental curve, which is the envelope of the first cycle responses obtained by Calvi and Bolognini[31] and the numerical response obtained by Bolis et al.[8] using the finite-element analysis software FEAP.[40] The load-displacement curves (experimental and numerical) are plotted for a horizontal displacement up to 110 mm, which corresponds to 4% inter-storey drift. A satisfactory agreement is observed although the initial stiffness of the system is slightly overestimated by the proposed model. This may be due the assumption of a rigid bond between the steel reinforcement and the concrete. Figure 6B shows the cyclic response of the bare frame obtained using the proposed modelling approach (BF_CY) compared to the experimental response[31] and the monotonic response (BF_MO).

Figure 7A illustrates and compares the experimental and numerical force-displacement curves of the traditional infilled frame subjected to monotonic loading (TIF_MO). Again, the proposed model describes with accuracy the initial as well as the post-peak behaviour of the system, up to a displacement of 25 mm. Beyond this value, both the proposed model and the model developed by Bolis et al.[8] exhibit a hardening behaviour. Table 7 compares the initial elastic stiffness K_e (i.e.

secant stiffness to the point at 40% of the peak load) and the peak load (F_{max}) according to the proposed model, the FE model of Bolis et al.,[8] and the experimental tests.[31] The proposed model overestimates the experimental elastic stiffness by 21.55% as compared to 16.21% estimated by Bolis et al.[8] Moreover, the proposed model estimates the peak load quite accurately (< 1% deviation) whereas the FE model of Bolis et al[8] overestimates the peak load by 11.20%.

Figure 7B illustrates the hysteretic response of the bare and of the infilled frame (TIF_CY). It can be observed that after a few cycles of deformation, the response of the infill frame tends to that of the bare frame due to the progressive damage accumulated in the infill. The response of the TIF_CY model is compared with that of the bare frame (BF_MO) and of the infilled frame (TIF_MO) under monotonic loading. A significant degradation of stiffness and a progressive reduction of strength is observed due to cyclic loading. This kind of behaviour strongly influences the earthquake response of infilled frame structures.

3.2 | Case study II: Frame with infill and sliding joints (after Bolis et al.[8])

The capability of the proposed modelling approach to describe the behaviour of an infill with sliding joints is assessed here considering the numerical tests carried out by Bolis et al.[8] on the RC frame of Calvi and Bolognini[31] infilled with two different types of panels, namely a traditional one and an innovative one with sliding joints (Figure 8A). The infill consists of a 14-course hollow clay brick (Figure 8A) masonry panel arranged in a running bond pattern laid such a way that the hole axes are parallel to the vertical direction (Figure 8B). The bed joints and head joints are fully filled with 10 mm thick mortar. In the case of the innovative infill, the vertical and horizontal sliding joints are made using wooden boards and polyethylene sheets that reduce the friction between the boards and the masonry. The horizontal joints (Figure 8C) divide the infill in four subpanels. Figure 8D illustrates the sliding vertical joints, which also present a shear key to transfer to the columns the out-of-plane forces acting on the infill.

The properties of the macro-elements, describing the infill subpanels and the joints, are calibrated using the results from the material tests presented in Bolis et al.[41] Tables 8-10 show the mechanical parameters characterising the normal and shear responses of the contact links, the infill-frame interfaces and the diagonal link, for the case of traditional infill.

Figure 9A shows the force-displacement curves for the RC frame with traditional infill under monotonic loading by Bolis et al.[8] and according to the proposed modelling strategy (TIF). Different discretisations of the masonry panel are considered in addition to the case of a single macro-element. These include the case of a mesh of 4 macro-elements along the vertical direction (4 × 1 mesh) as in Figure 2C and the case of a 4 × 2 mesh as in Figure 2D.

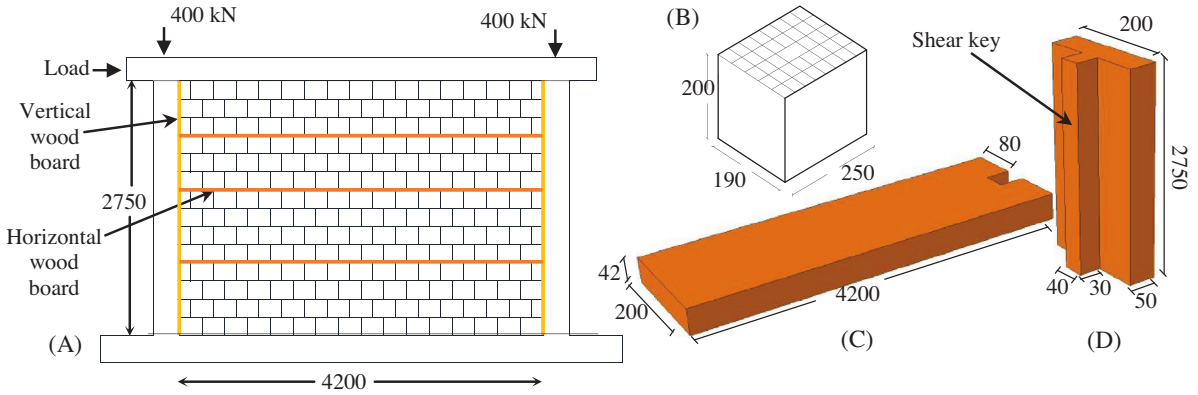

FIGURE 8 Infilled frame incorporating the proposed construction technique showing the connection details (A) Infill with sliding mechanism, (B) hollow clay brick, (C) horizontal wooden board, (D) lateral wooden board (measures in mm)

TABLE 8 Mechanical parameters of the masonry for defining the contact normal links

	E_m (MPa)	f_{cm} (MPa)	f_{tm} (MPa)	f_{rm} (MPa)	ε_{cu} (-)	ε_{tu} (-)	λ (-)	Source
Horizontal	4408	2.70	0.52	0.54	0.4	0.0030	0.1	[8,41]
Vertical	16148	7.28	0.63	1.52	0.4	0.0008	0.1	[8,41]

TABLE 9 Mechanical parameters of the contact links in shear describing the frame-infill interaction

Interaction Properties	CM	BBM	TBM	PPH	PPV	Source
k_j (N/mm^3)	150	200	100	200	150	Proposed model
c_j (MPa)	0.20	0.41	0.20	0.41	0.41	[8,41]
μ_j (-)	0.75	0.85	0.75	0.85	0.75	[8,41]

TABLE 10 Mechanical parameters for defining the response envelope of the diagonal link

G_m(MPa)	τ_{cr}(MPa)	τ_y(MPa)	τ_0(MPa)	τ_r(MPa)	γ_{cr}(-)	γ_y(-)	γ_0(-)	γ_r(-)	Source
2998	0.468[a]	0.654[a]	0.720	0.072[a]	0.0002[a]	0.0022[a]	0.0043[a]	0.0216[a]	[8,41]

[a]This parameter has been evaluated to provide by fitting the experimental results.

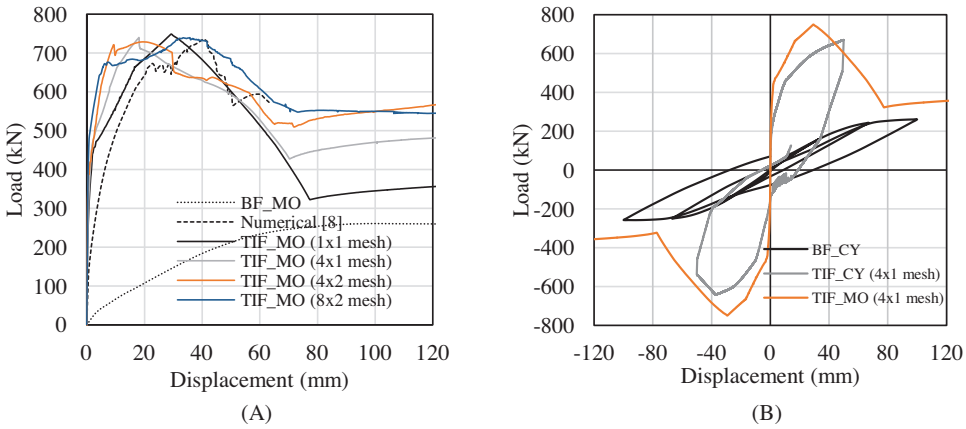

FIGURE 9 Comparison of numerical responses of the RC frame with traditional infill under (A) monotonic loading and (B) cyclic loading predicted by various modelling approaches

The numerical response of the bare frame obtained by Bolis et al.[8] is also shown in the figure for comparison. The proposed models provide results that are in quite good agreement with the results obtained with the more computationally expensive model of Bolis et al.[8] Moreover, the global response of the system is not significantly affected by the infill mesh discretisation. Increasing the number of elements, the model maintains the same initial stiffness and the same strength, whereas a slightly different stiffness can be observed in the nonlinear response as well as in the residual strength. Figure 9B shows the hysteretic response of the system with traditional infills, evaluated by imposing cyclic displacement inputs with increasing amplitude. The cyclic response of the infilled frame (TIF_CY) is compared with the cyclic response of the bare frame (BF_CY) and the monotonic capacity curve of the infilled frame (TIF_MO). A slight reduction in terms of lateral stiffness and peak load is observed due to the degradation under cyclic loading.

The normal behaviour of the sliding joints is defined by the initial normal stiffness per unit area $k_{nj} = 60.7$ N/mm^3, the tensile strength $f_{tj} = 0$ MPa and the compressive strength $f_{cj} = 6.74$ MPa. The values of the mechanical parameters of the masonry subpanel defining the contact normal links properties are presented in Table 11. Table 12 report the properties of the joints defining the contact normal links and contact interfaces for the case of the modified masonry infill with the sliding joints (SJ), corresponding to model J3.LB in Bolis et al.[8]

Figure 10A shows the monotonic response obtained by Bolis et al.[8] and the responses obtained with the proposed modelling approach using a 4 × 1, 4 × 2 and a 8 × 2 mesh for the infill (IFSJ_MO). It can be observed that the addition of the sliding joints enhances the compliance of the system compared to the frame with traditional infills, with a response

TABLE 11 Mechanical parameters of the masonry for defining the contact normal links

	E_m (MPa)	f_{cm} (MPa)	f_{tm} (MPa)	f_{rm} (MPa)	ε_{cu} (-)	ε_{tu} (-)	λ (-)	Source
Horizontal	3275	2.70	0	0.54	0.4	0.010	0.1	[8,41]
Vertical	2111	7.28	0	1.52	0.4	0.002	0.1	[8,41]

TABLE 12 Mechanical parameters of contact links in shear describing the frame-infill interaction

	CM	BBM	TBM	PPH(SJ)	PPV	Source
k_j (N/mm^3)	85	100	100	36	100	[8,41]
c_j (MPa)	0.020	0.4	0.2	0.020	0.4	[8,41]
μ_j (-)	0.42	0.85	0.75	0.42	0.42	[8,41]

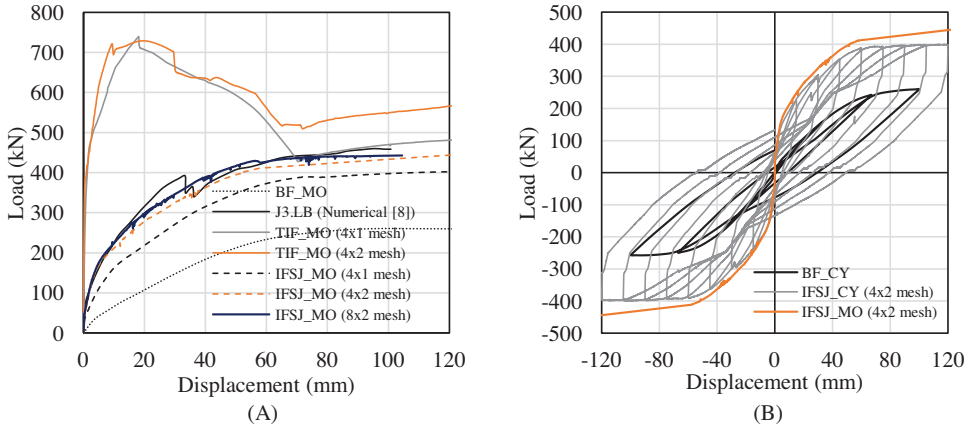

FIGURE 10 Numerical response of the RC frame with masonry infill and sliding joint under (A) monotonic loading and (B) cyclic loading

that is closer to the one of the bare frame than to the infilled one. The load-displacement curves obtained by the 4 × 2 and 8 × 2 meshes are very close and result in a good agreement with the numerical results reported in Bolis et al.[8] Some differences are observed in the non-linear response of the 4 × 1 model. However, the deviation in terms of the ultimate load is less than 10%. These results confirm the capability of the proposed approach of describing the global response of infilled frames equipped with sliding joints, even employing a limited number of contact links along the column or beam lengths.

Figure 10B shows the cyclic response of the frame with infill and sliding joints (IFSJ_CY), compared to the monotonic capacity curve obtained with the 4 × 2 mesh (IFSJ_MO) and the cyclic response of the bare frame (BF_CY). The presence of the sliding joints strongly reduces the initial stiffness and the strength of the infilled frame. Furthermore, the system IFSJ_CY exhibits stable and good cyclic dissipative properties thanks to the frictional behaviour in correspondence of the sliding joints and this is expected to have beneficial effects for the seismic performance of the system.

Figure 11 illustrates the deformed shapes of the models TIF and IFSJ with different discretisations of the infill, for a displacement of 55 mm, corresponding to a 2% inter storey drift ratio. These are found to be consistent with the deformed shapes obtained by Bolis et al.[8] using a 2D modelling approach. The figures show also the contact normal links that are active in compression, thus helping to visualize the location where the infill subpanels are in contact with the frame.

It is worth noting that the joints do not completely avoid the flexural interaction between the infill and the surrounding frame. However, they provide a significant reduction of the overall stiffness and strength of the system and prevent the damage in the masonry panels, leading to a regular and dissipative cyclic response whose beneficial effects should be better investigated through experimental cyclic and dynamic analyses. Furthermore, the avoidance of the in-plane damage of the masonry panels is expected to provide a better behaviour also with respect to out-of-plane actions, which are not investigated in the present work.

In order to shed light on how the different infill typologies affect the responses of the RC frame components, the axial force, shear force and bending moment on the left (windward) and right (leeward) column are evaluated for the BF, TIF (4 × 1 mesh) and IFSJ models (4 × 1 mesh). Their diagrams are illustrated in Figure 12–14, respectively, where (z/H) denotes the distance of the cross-section from the base of the column normalised by the column length. The reported diagrams refer to inter-storey drifts (ISD) of 0% (i.e., before application of lateral load), and 2%. The shape of the diagrams is characterised by discontinuities due to the forces transferred by the 2D contact links to the columns. It can be observed in Figure 12 that the axial force distribution in the two columns is almost uniform when the frame is subjected to zero or very low drift angles, as expected. At higher drift levels, the axial force distribution slightly changes showing an increased axial force

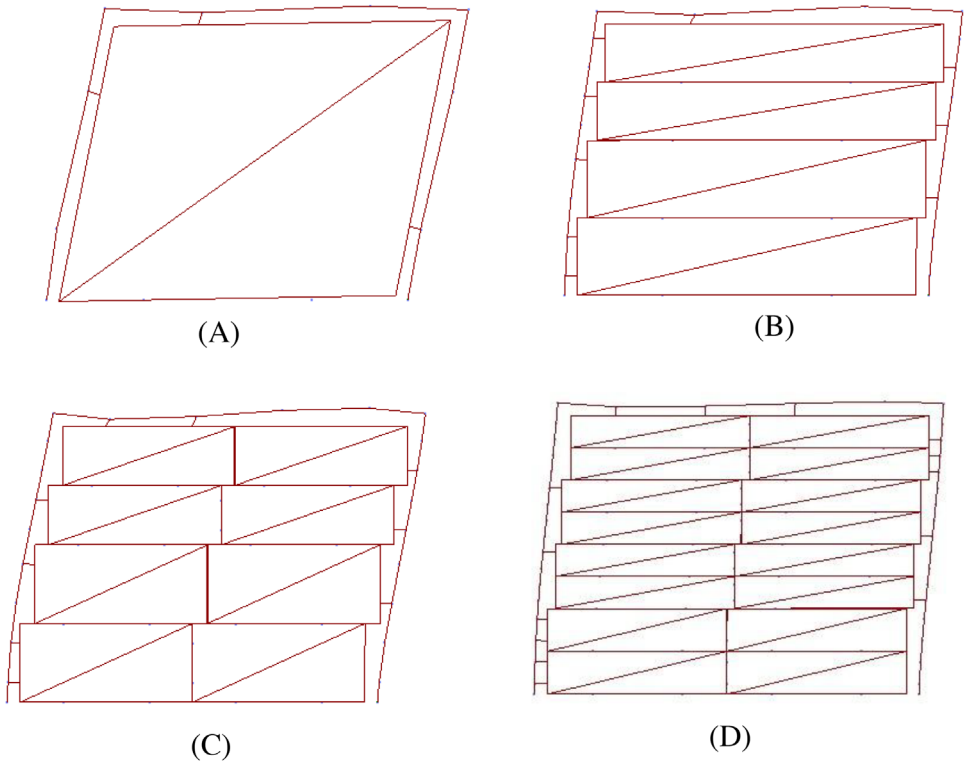

FIGURE 11 Deformed shapes of (A) TIF, (B) IFSJ (4 × 1 mesh), (C) IFSJ (4 × 2 mesh), (D) IFSJ (8 × 2 mesh)

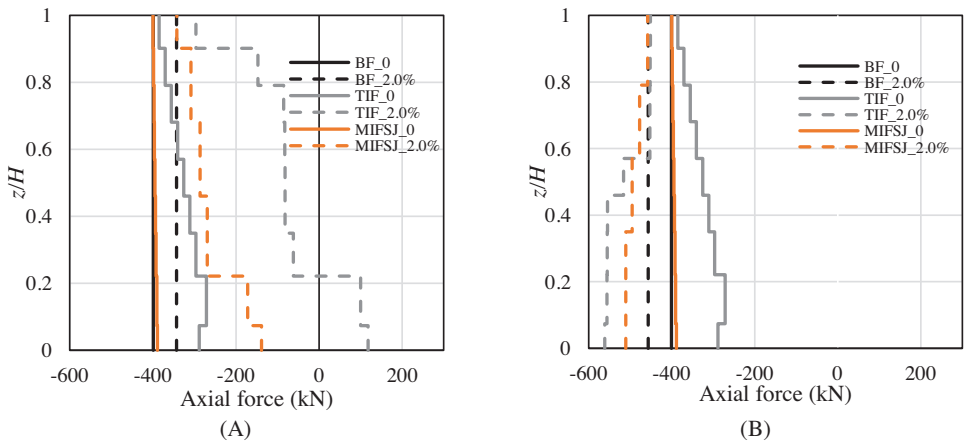

FIGURE 12 Comparisons of axial forces in BF, TIF (4 × 1 mesh) and IFSJ (4 × 1 mesh) for (A) windward column (B) leeward column

(compressive) at the base of the leeward column and a decrease in the windward one, due to the transfer of tangential forces by the macro-elements and the effect of the overturning moment generated by the horizontal force eccentric with respect to the ground. At 2% drift, in the windward column, the highest values of the compressive force are observed in the BF system, and the lower in the TIF system. In the leeward column, the compressive forces are highest in the TIF system and lowest in the BF system.

Figure 13 shows the shear force diagrams of the columns. These diagrams are characterised by the discontinuities caused by the transmission of the normal forces in the 2D contact links. It is possible to observe that the sliding joints are effective in reducing the shear forces in the IFSJ system compared to the TIF system. However, the reduction is more significant in the leeward column than in the windward column. The distribution of the bending moments, shown in Figure 14, is approximately linear when only vertical loads are applied. Under a drift of 2%, the values of the maximum bending

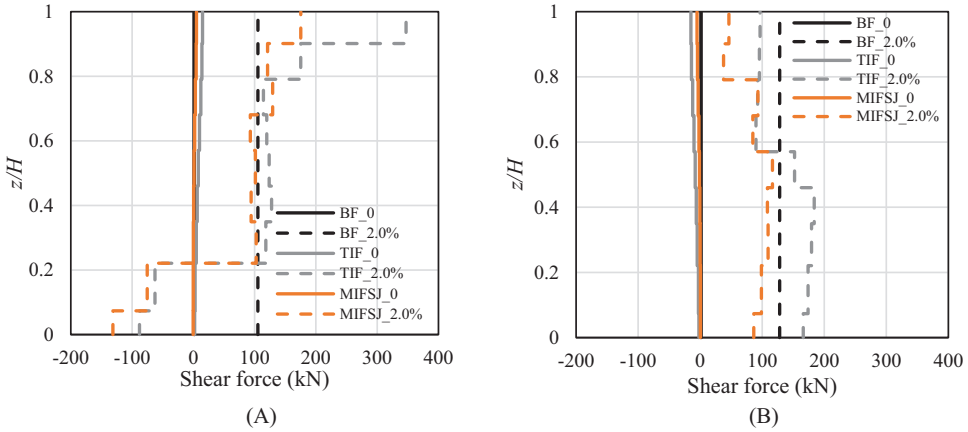

FIGURE 13 Comparisons of shear forces in BF, TIF (4 × 1 mesh) and IFRJ (4 × 1 mesh) for (A) windward column (B) leeward column

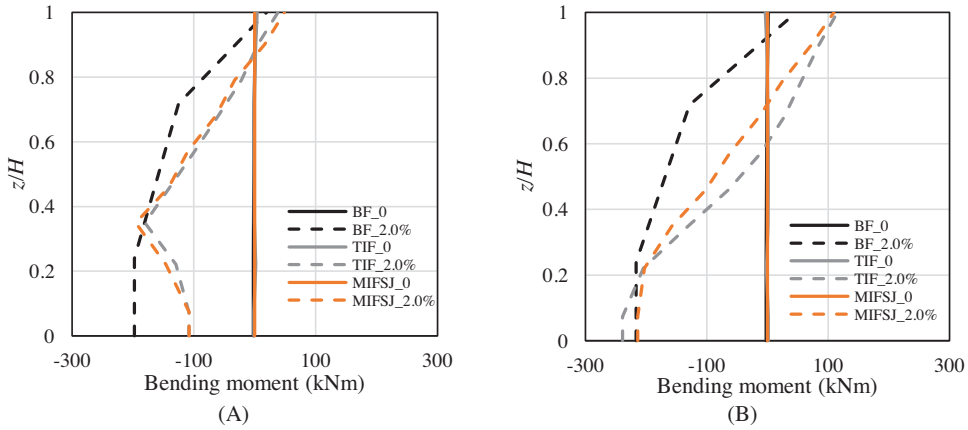

FIGURE 14 Comparisons of bending moments in BF, TIF (4 × 1 mesh) and IFSJ (4 × 1 mesh) for (A) windward column (B) leeward column

moments for the various systems are comparable, and they are generally higher for the BF model in the windward column and for the TIF model in the leeward column.

3.3 | Case study III (INSYSME Project[32])

The final validation study is carried out on the prototypes tested by the University of Padova within the INSYSME project[32] and further described in Verlato.[33] The experimental outcomes for the bare frame, the infilled frame with mortar joints only (FC. MJ, 4th frame specimen) and the infilled frame with both mortar and specially designed rubber joints (DRES-V2) are validated against the proposed macro-modelling strategy. Hollow clay masonry blocks with a hole percentage of 50% (D-type) were used to build the infill panel. The masonry blocks were arranged in a running bond pattern and laid such a way that the hole axes are parallel to the vertical direction (Figure 15A). A mortar of 10 mm thickness was used in the bed joints, whereas there are no mortar present in the head joints and the transfer of stresses from between adjacent blocks relied on the brick inter-locking. Details of the frame cross sections, rebar diameter and detailing scheme, are given in Figure 15B together with the masonry block dimensions and further details are available in.[33] A constant vertical load of 200 kN was applied at the top of the column (simulating the effect of permanent load acting on the RC frame) and the experimental quasi-static tests conducted on the bare frame, the traditional infilled frame with mortar joints only and the innovative infill with both mortar and rubber joints followed by monotonically increasing in-plane horizontal load applied at the end of the beam (see Figure 15A).

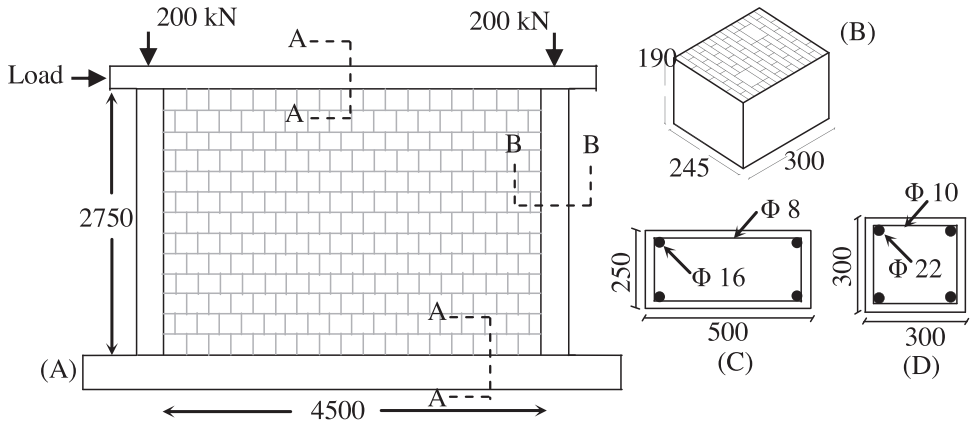

FIGURE 15 Geometric details (dimensions in mm) of (A) the tested infilled frame, (B) the perforated clay block (brick unit), (C) top and bottom beam (section A-A), (D) column (section B-B)

TABLE 13 Mechanical properties of concrete and reinforcing steel

Mechanical properties	Concrete	Steel reinforcement	Source
E (MPa)	22000	180000	[32,33]
ν (-)	0.15	0.3	[32,33]
f_c (MPa)	40	–	[32,33]
Yield strength (MPa)	–	535	[32,33]
f_t (MPa)	3.9	–	[32,33]
Post-elastic to elastic stiffness ratio	–	0.002	[32,33]

TABLE 14 Mechanical parameters of the masonry for defining the contact normal links

Direction	E_m (MPa)	f_{cm} (MPa)	f_{tm} (MPa)	f_{rm} (MPa)	ε_{cu} (-)	ε_{tu} (-)	λ (-)	Source
Horizontal	1904	1.40	0.1	0.28	0.4	0.001	0.1	[32,33]
Vertical	6158	7.63	0.52	1.52	0.4	0.001	0.1	[32,33]

Table 13 reports the main mechanical properties of the concrete and steel reinforcement employed for the frame components. The mechanical parameters of the normal and shear responses of contact links and the response envelope of the diagonal links are presented in Table 14, Table 15 and Table 16, respectively. The constitutive parameters of the shear contact links, namely those describing the macroscopic sliding behaviour of masonry in the horizontal (PPH) and vertical (PPV) directions, the column-infill (CM) and beams-infill (BBM, TBM) interfaces, are assumed according to[33] The constitutive behaviour of the contact links describing the interaction between the panel and the columns simulates the presence of mortar in the vertical joints.

Figure 16A compares the horizontal force-displacement response of the bare frame under monotonic loading obtained in INSYSME[32] with the ones obtained numerically by Verlato[33] using a 2D plane stress model and by using the proposed

TABLE 15 Mechanical parameters of the contact shear links describing the masonry sliding behaviour and the frame-infill interaction

Interaction Properties	CM	BBM	TBM	PPH	PPV	Source
k_j (N/mm^3)	100	100	100	100	100	Proposed model
c_j (MPa)	0.41	0.41	0.1	0.41	0.41	[32,33]
μ_j (-)	0.8	1.13	0.4	1.13	0.8	[32,33]

TABLE 16 Mechanical parameters of the response envelope of the diagonal link

G_m, (MPa)	τ_{cr}(MPa)	τ_y, (MPa)	τ_0(MPa)	τ_r(MPa)	γ_{cr}(-)	γ_y(-)	γ_0(-)	γ_r(-)	Source
1175	0.201[a]	0.281[a]	0.310	0.031[a]	0.0002[a]	0.0020[a]	0.0040[a]	0.0277[a]	[32,33]

[a]This parameter has been evaluated to provide by fitting the experimental results.

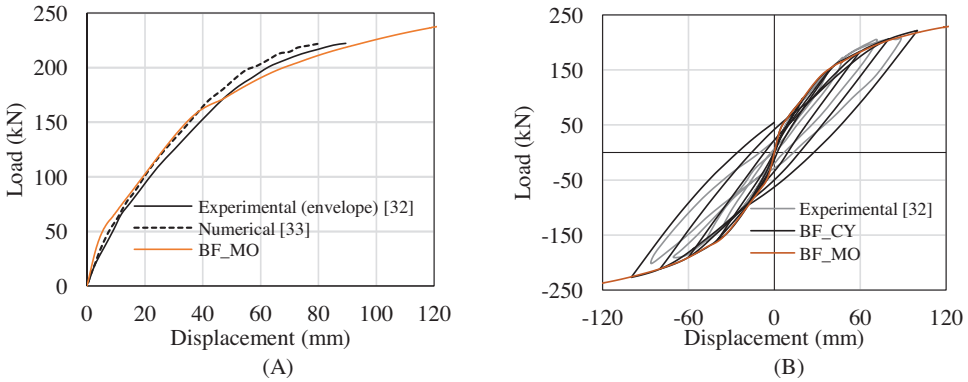

FIGURE 16 Comparison between numerical and experimental load-displacement curves of bare frame under (A) monotonic and (B) cyclic loading

modelling strategy. The experimental and numerical force-displacement curves are plotted for a horizontal displacement up to 110 mm, corresponding to an inter-storey drift of 4%. The overall agreement between the numerical and experimental curves is good, although the numerical models slightly overestimate the initial stiffness of the system. Again, this may be due to the assumption of rigid bond between rebars and concrete. Figure 16B compares the experimental and numerical curves obtained under a cyclic loading. The proposed model is characterised by a slightly larger hysteresis compared to the one observed in INSYSM.[32]

3.3.1 | Frame with traditional infill

Figure 17A illustrates the experimental force-displacement curve of the infilled frame under monotonic loading and compares it with the one obtained numerically (TIF_MO) considering different infill discretisations. Again, the proposed models describe with good accuracy both the initial and the post-peak behaviour of the wall. Increasing the number of macro-elements for describing the infill results in a slightly increase of stiffness and strength. A good agreement is also observed between the cyclic responses (Figure 17B).

3.3.2 | Infill frames with rubber joints

Figure 18A shows the layout of the RC frame with the infill panel and rubber joints. The rubber joints used as horizontal layers are 15 mm thick and have a special shape to achieve a different stiffness in the two horizontal directions[13] (Figure 18B)

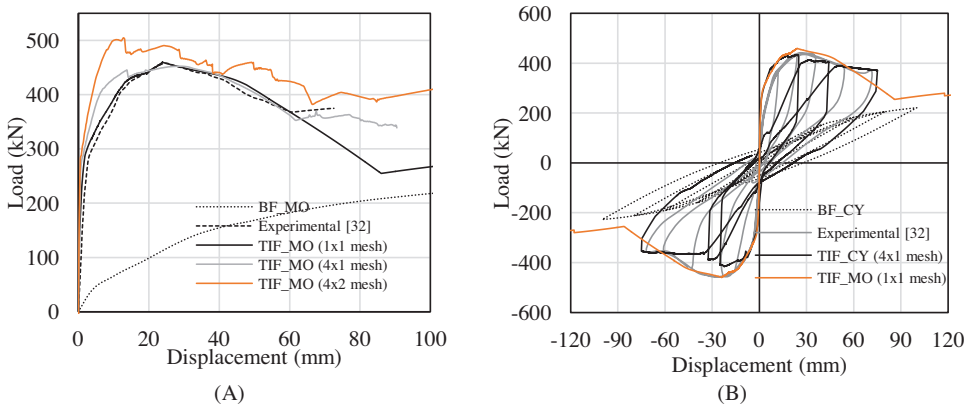

FIGURE 17 Comparison between numerical responses of infilled frame with single and multi-panel approach and validation against experimental load-displacement curves for (A) monotonic and (B) cyclic loading

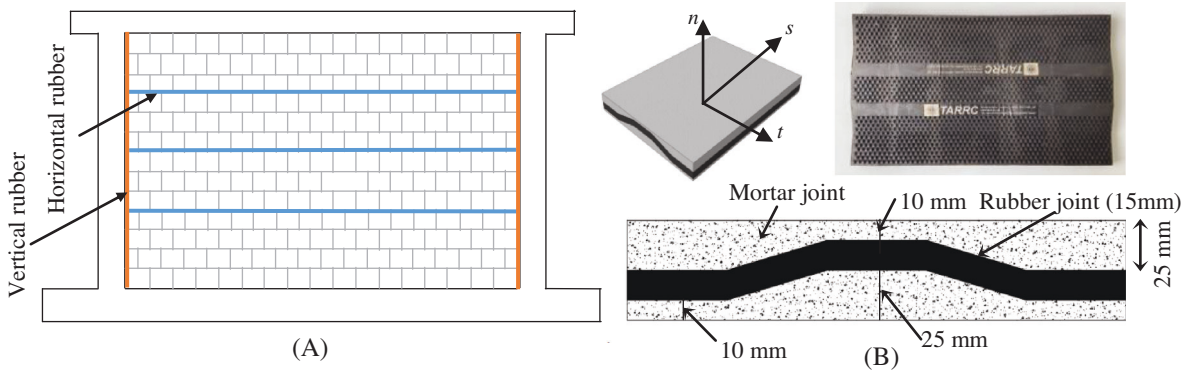

FIGURE 18 (A) Masonry infilled walls with horizontal and vertical rubber joints; (B) rubber joints developed by TARRC [13]

TABLE 17 Mechanical parameters of the masonry for defining the contact normal links

Direction	E_{rj} (MPa)	k_{nj} (N/mm^3)	f_{cj} (MPa)	f_{tj} (MPa)	ε_{cu} (-)	ε_{tu} (-)	λ (-)	Source
Horizontal	3275	200	1.40	0	0.4	0.001	0.1	32,33
Vertical	2111	200	1.58	0	0.4	0.001	0.1	32,33

TABLE 18 Mechanical parameters of contact links in shear for the various interfaces

Interaction Properties	CM	BBM	TBM	PPH(RJ)	PPV	Source
k_j (N/mm^3)	1.00	100	100	11.73	100	36
c_j (MPa)	0.001	0.4	0.1	0.05	0.3	32,33
μ_j (-)	0.3	1.13	0.4	0.36	0.4	32,33

and are laid with mortar joints between them and the bricks. This rubber joint is made with natural rubber compound and possess a shear modulus of 0.5 MPa. The vertical rubber layers present between the infill and the columns are made with a different compound prepared from recycled Styrene-Butadiene Rubber and Ethylene Propylene Diene Monomer rubber anchored to a support of non-woven fabric. The normal behaviour of the horizontal rubber joints is defined by the initial normal stiffness $k_{nj} = 11.73$ N/mm^3, the tensile strength $f_{tj} = 0$ MPa and the compressive strength $f_{cj} = 1.58$ MPa. The properties of the modified masonry infill and contact interfaces describing the mortar-rubber-mortar joints are presented in Table 17 and Table 18. The data reported in Tables 13–18 are based on the tests carried out by INSYSME[32] and numerical models developed by Verlato[33] to simulate these tests.

Figure 19A compares the experimental force-displacement curve with the ones obtained numerically considering two different discretisations of the infill with joints, based on a 4 × 1 and 4 × 2 mesh for the infill. The proposed models

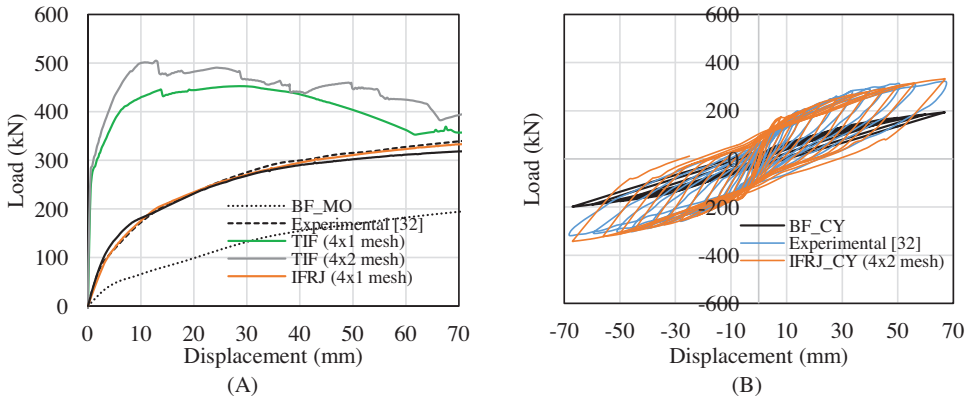

FIGURE 19 Comparison between numerical responses of the bare frame, infilled frame with traditional infills and infill with innovate joints (rubber joints) for (A) monotonic and (B) cyclic loading

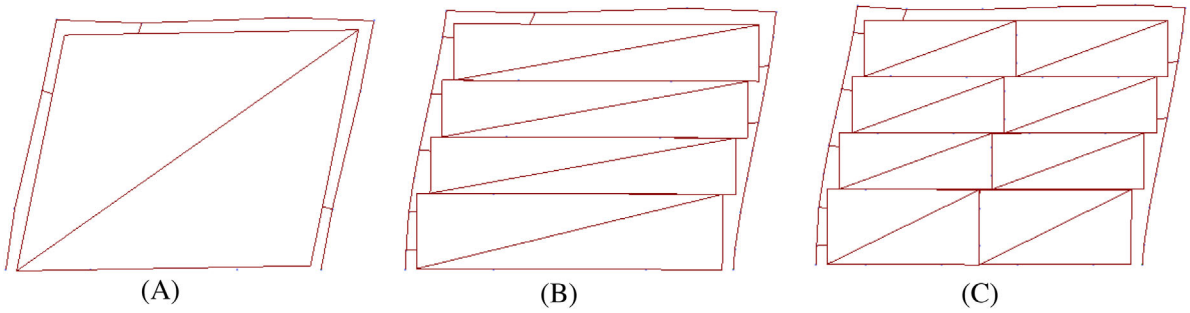

FIGURE 20 Deformed shapes of (A) TIF (B) IFRJ (4 × 1 mesh) (D) IFRJ (4 × 2 mesh)

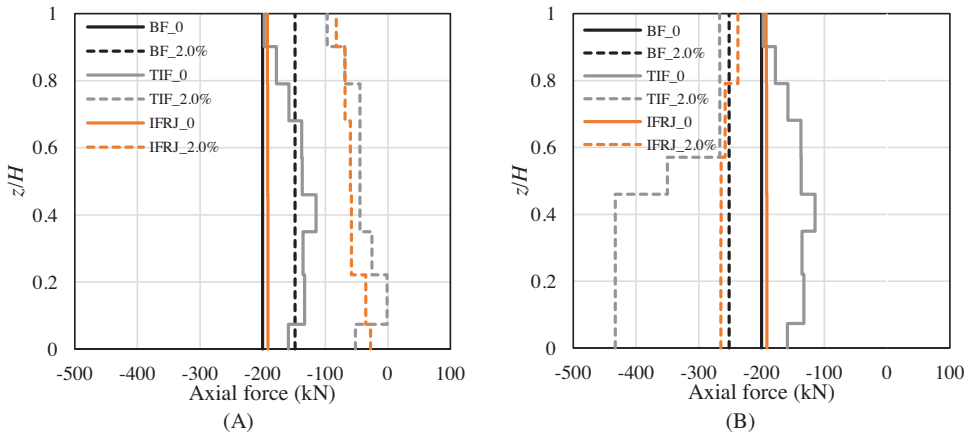

FIGURE 21 Comparisons of axial forces in BF, TIF (4 × 1 mesh) and IFRJ (4 × 1 mesh) for (A) windward column (B) leeward column

provide accurate results, with a global force-lateral displacement curve very close to the experimental one. This is despite the use of a simplified model for the shear behaviour of the mortar-rubber joints. Very good results are obtained because the proposed model is able to accurately simulate the failure of the bond between the rubber joints and the mortar layers that was experienced in the tests for rather low drift levels, and the sliding behaviour taking place following the interface failure. Increasing the number of macro-elements results in only a slight increase of stiffness of the system. The addition of the rubber joints is found to enhance the compliance of the system, compared to the case of traditional infills (Figure 17A). Figure 19B shows the cyclic response of the system according to the experiment[32] and the numerical model with a 4 × 2 mesh for the infill. The agreement between the two is quite good. The system with rubber joints is found to be beneficial with significant energy dissipation capacity and stable loops. Figure 20 illustrates the deformed shape of the TIF model and two infilled frames with rubber joint (IFRJ) for different discretisations, for a 2% inter storey drift. These are found to be consistent with the experimental results obtained by Verlato.[33]

The axial force, shear force and bending moment on the windward and leeward column are evaluated for the BF, TIF (4 × 1 mesh) and IFRJ models (4 × 1 mesh). Their diagrams are illustrated in Figures 21–23, respectively, and they are quite similar in shape to those obtained for the model with sliding joints (Figures 12–14). Thus, similar observations hold for this case.

Figure 22 shows the shear force diagrams of the columns. These diagrams are characterised by the discontinuities caused by the transmission of the normal forces in the 2D contact links. It is possible to observe that the rubber joints are effective in reducing the shear forces in the IFRJ system compared to the TIF system. However, the reduction is more significant in the leeward column than in the windward column. The distribution of the bending moments, shown in Figure 23 is approximately linear when only vertical loads are applied. Under a drift of 2%, the values of the maximum bending moments for the various systems are comparable, and they are generally higher for the BF model in the windward column and for the TIF model in the leeward column.

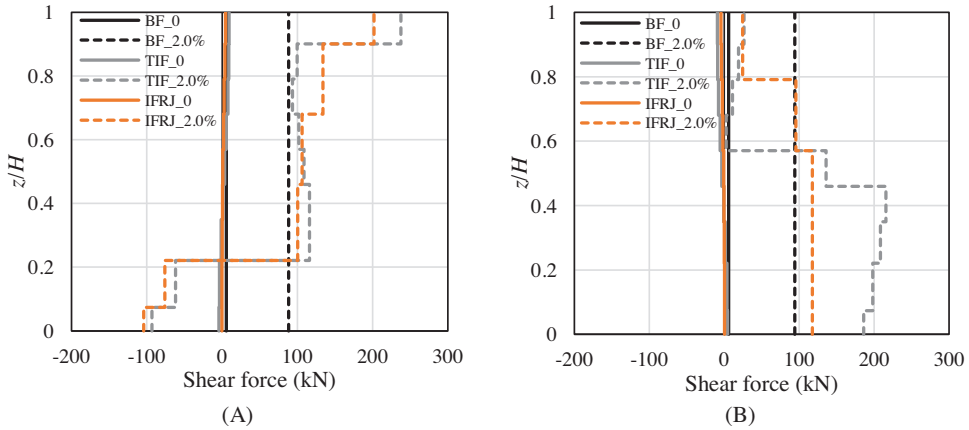

FIGURE 22 Comparisons of shear forces in BF, TIF (4 × 1 mesh) and IFRJ (4 × 1 mesh) for (A) windward column (B) leeward column

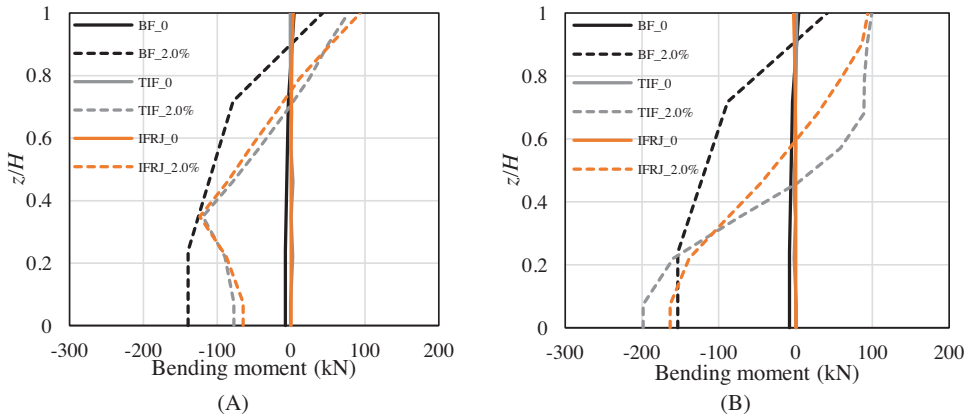

FIGURE 23 Comparisons of bending moments in BF, TIF (4 × 1 mesh) and IFRJ (4 × 1 mesh) for (A) windward column (B) leeward column

Figure 24A and Figure 24B show and compare the diagonal spring force (F_d) versus diagonal spring elongation (d_d) in each of the subpanel used to discretise the masonry infill in the cases of traditional infill (Figure 24A) and infill with rubber joint (Figure 24B), where SP_1 denotes the bottom subpanel and SP_4 the top. In case of TIF, all the subpanels are found to be significantly damaged, with the exception of SP_4, whereas in the IFRJ case the diagonal spring behave linearly without any visible diagonal failure. It is also interesting to observe that SP_1 and SP_3 undergo unloading, whereas SP_2 does not unload and enters into the softening regime. This corresponds to a change in the deformed shape of the frame, with horizontal deflections localised in correspondence of SP_2. Obviously, with a simpler modelling approach using an equivalent strut for representing the infills, such a behaviour would not be simulated.

Figure 24C and Figure 24D show the forces in the diagonal links versus the top displacement of the frame. The relationship is nonlinear even in the case of linear behaviour of the diagonal links due to the nonlinear relationship between diagonal displacements of the panels and drifts. These two figures are useful to better highlight that the subpanels attain the peak load and undergo a softening behaviour in the traditional infills whereas they do not reach the peak load in the case of infills with rubber joints. Figure 25 compares the experimental and numerical values of the secant stiffness and of the dissipated energy. The secant stiffness is defined as the ratio between the force at the maximum displacement of each cycle and the displacement amplitude. The energy dissipated is the cumulative energy obtained by integrating the force-displacement curve. The proposed model provides quite good estimates of the secant stiffness, which is only slightly overestimated for displacement amplitudes up to 10 mm. Moreover, the model also underestimates the dissipated energy at small displacements amplitudes and overestimates it for larger ones.

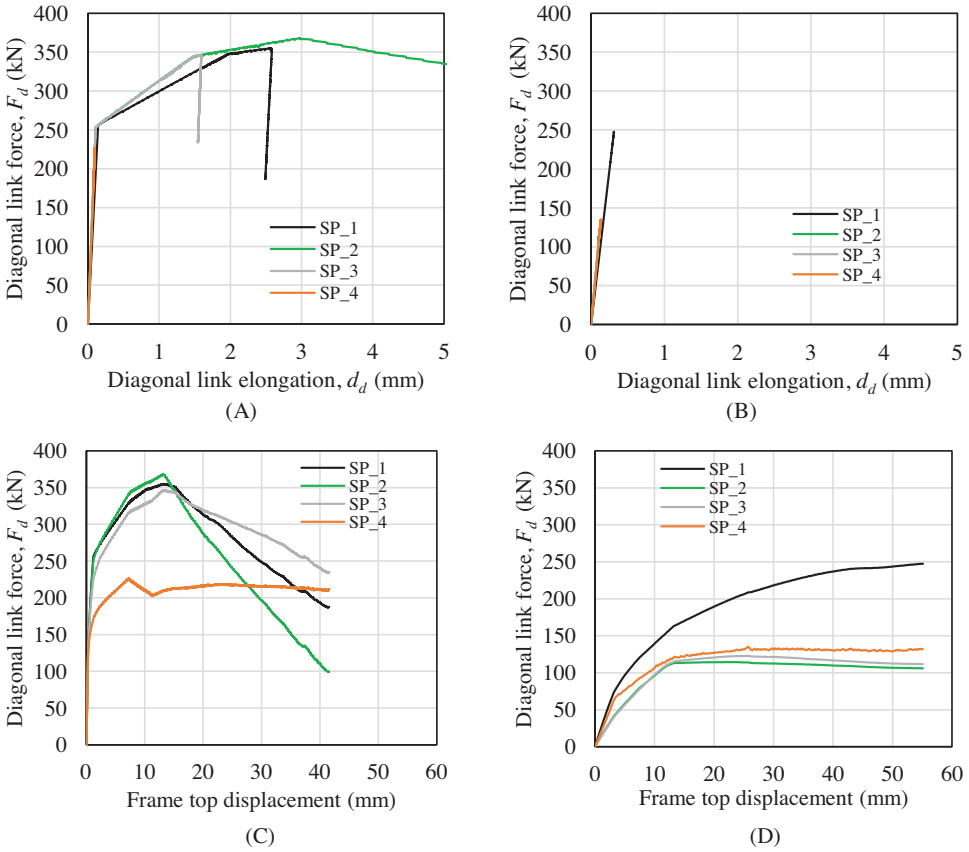

FIGURE 24 Internal force in the diagonal link against the diagonal link elongation: (A) TIF, (B) IFRJ; and against the top frame displacement: (C) TIF, (D) IFRJ.

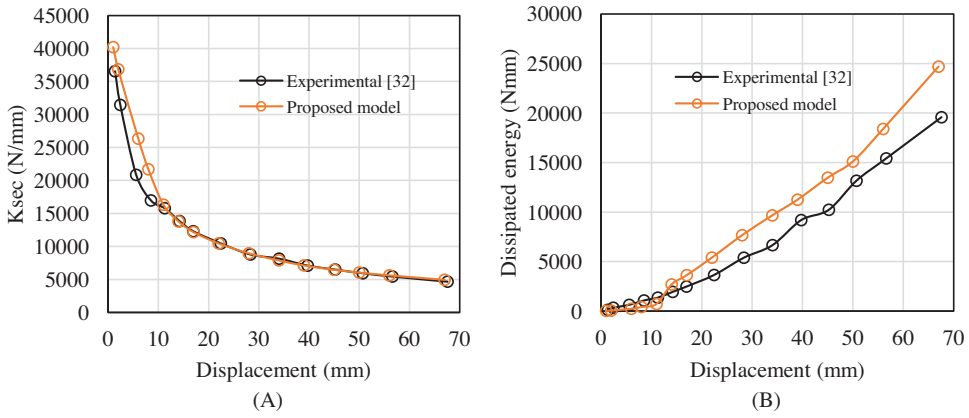

FIGURE 25 Comparison of experimental and numerical (A) secant stiffness and (B) dissipated energy

4 | CONCLUSION

This paper has proposed an innovative and computationally efficient approach for analysing the in-plane non-linear cyclic response of RC frames with masonry infills and flexible/sliding joints. The proposed approach is based on a fibre-element based description of the frame components, and with the use of 2D discrete macro-elements, implemented in OpenSees, for describing the behaviour of the masonry subpanels and the interaction between them and with the adjacent frame components. The modelling strategy allows to evaluate the effectiveness of the sliding joints and rubber joints in

minimising the negative effects of the interaction between infill and RC frame, by shedding light not only on their impact on the global force-displacement behaviour of the system, but also on the internal forces in the individual components.

The proposed modelling approach is calibrated and validated based on experimental test results and numerical results obtained by more refined FEM models available in the literature. Based on the study outcomes, the following conclusions can be made:

- the addition of the sliding/flexible joints enhances the compliance of the infilled frames, with a response that is closer to the one of the bare frames than of traditionally infilled ones. The energy dissipation capabilities are also enhanced thanks to more stable and larger hysteresis loops under cyclic loading;
- the proposed modelling strategy describes with good accuracy the initial as well as the post-peak force-displacement response of the analysed systems under horizontal loading;
- the global response of the system is not significantly affected by the infill mesh discretisation. Increasing the number of elements, the model becomes slightly stiffer and also the residual strength increases.
- for a given level of drift demand, the internal forces in the columns of the RC frame with infill and rubber joints have maximum values similar, if not inferior to those of the bare frame, with the exception of the axial and shear force in the windward column. The maximum absolute values of the internal forces in the case of infill with rubber joints are lower than the corresponding values obtained in the system with traditional infill.

In conclusion, the proposed modelling strategy can be effectively employed to investigate the optimal combination of strength, deformability and dissipation capacity of the sliding/flexible joints for enhancing the seismic performance for a wide variety of infilled frames. Further analyses will be carried out to evaluate the contribution of the sliding/flexible joints to the energy dissipation capabilities of infilled frames and to analyse the dynamic behaviour and seismic response of more complex structural systems.

ACKNOWLEDGMENTS

We are thankful to the Department of Civil and Environmental Engineering at the University of Strathclyde for providing the computational resources to carry out the numerical analyses.

DATA AVAILABILITY STATEMENT

The data used to support the findings of this study are available from the corresponding author upon request.

ORCID

Prateek Kumar Dhir https://orcid.org/0000-0003-3803-1913
Enrico Tubaldi https://orcid.org/0000-0001-8565-8917
Bartolomeo Pantò https://orcid.org/0000-0002-3340-228X
Ivo Caliò https://orcid.org/0000-0002-8063-8359

REFERENCES

1. Del Vecchio C, Di Ludovico M, Pampanin S, Prota A. Repair costs of existing rc buildings damaged by the l'aquila earthquake and comparison with FEMA P-58 predictions. *Earthq Spectra*. 2018;34(1):237-263. https://doi.org/10.1193/122916EQS257M
2. De Risi MT, Del Gaudio C, Verderame GM. Evaluation of repair costs for masonry infills in RC buildings from observed damage data: the case-study of the 2009 L'Aquila earthquake. *Buildings*. 2019;9(5):122. https://doi.org/10.3390/buildings9050122
3. Elgawady M, Lestuzzi P, Badoux M. A review of conventional seismic retrofitting techniques for URM. *13th International Brick and Block Masonry Conference*. 2004:1-10. [Online]. Available http://imacwww.epfl.ch/GenieParasismique/EDOC_ST09/Course_6/old/89ElGA13-IBMaCstateoftheart.pdf
4. Koutas L, Bousias SN, Triantafillou TC. Seismic Strengthening of Masonry-Infilled RC Frames with TRM: experimental Study. *J Compos Constr*. 2015;19(2):04014048. https://doi.org/10.1061/(asce)cc.1943-5614.0000507
5. Morandi P, Milanesi RR, Magenes G. Innovative seismic solution for clay masonry infills with sliding joints: principles and details. *Brick Block Mason. Trends, Innov. Challenges - Proc. 16th Int. Brick Block Mason. Conf. IBMAC 2016*. 2016:1273-1282. https://doi.org/10.1201/b21889-158
6. Preti M, Bettini N, Plizzari G. Infill walls with sliding joints to limit infill-frame seismic interaction: large-scale experimental test. *J Earthq Eng*. 2012;16(1):125-141. https://doi.org/10.1080/13632469.2011.579815
7. Preti M, Bolis V, Stavridis A. Seismic infill–frame interaction of masonry walls partitioned with horizontal sliding joints: analysis and simplified modeling. *J Earthq Eng*. 2019;23(10):1651-1677. https://doi.org/10.1080/13632469.2017.1387195

8. Bolis V, Stavridis A, Preti M. Numerical investigation of the in-plane performance of masonry-infilled RC frames with sliding subpanels. *J Struct Eng (United States)*. 2017;143(2):1-18. https://doi.org/10.1061/(ASCE)ST.1943-541X.0001651
9. Di Trapani F, Bolis V, Basone F, Preti M. Seismic reliability and loss assessment of RC frame structures with traditional and innovative masonry infills. *Eng Struct*. 2020;208(February):110306. https://doi.org/10.1016/j.engstruct.2020.110306
10. Preti M, Migliorati L, Giuriani E. Experimental testing of engineered masonry infill walls for post-earthquake structural damage control. *Bull Earthq Eng*. 2015;13(7):2029-2049. https://doi.org/10.1007/s10518-014-9701-2
11. Preti M, Bolis V. Masonry infill construction and retrofit technique for the infill-frame interaction mitigation: test results. *Eng Struct*. 2017;132:597-608. https://doi.org/10.1016/j.engstruct.2016.11.053
12. Vögeli C, Mojsilović N, Stojadinović B. Masonry wallettes with a soft layer bed joint: behaviour under static-cyclic loading. *Eng Struct*. 2015;86:16-32. https://doi.org/10.1016/j.engstruct.2014.12.038
13. Ahmadi H, Dusi A, Gough J, A Rubber-Based System for Damage Reduction in Infill Masonry Walls. 2017.
14. Mojsilović N, Petrović M, Anglada XR. Masonry elements with multi-layer bed joints: behaviour under monotonic and static-cyclic shear. *Constr Build Mater*. 2015;100:149-162. https://doi.org/10.1016/j.conbuildmat.2015.09.065
15. Calabria A, Guidi G, da Porto F, Modena C. Innovative systems for masonry infill walls based on the use of rubber joints: finite element modelling and comparison with in-plane tests. *Brick Block Mason. Trends, Innov. Challenges - Proc. 16th Int. Brick Block Mason. Conf. IBMAC 2016*. 2016:1155-1162. https://doi.org/10.1201/b21889-144
16. Petrović M, Mojsilović N, Stojadinović B. Masonry walls with a multi-layer bed joint subjected to in-plane cyclic loading: an experimental investigation. *Eng Struct*. 2017;143:189-203. https://doi.org/10.1016/j.engstruct.2017.04.025
17. Petrović M, Stojadinović B, Mojsilović N. I-Shaped Unreinforced Masonry Wallettes with a Soft-Layer Bed Joint: behavior under Static-Cyclic Shear. *J Struct Eng*. 2017;143(11):1-20. https://doi.org/10.1061/(ASCE)ST.1943-541X.0001884
18. Preti M, Nicola B, Laura M, Valentino B, Andreas S, Giovanni AP. Analysis of the in-plane response of earthen masonry infill panels partitioned by sliding joints. *Earthq Eng Struct Dyn*. 2016;45(8):1209-1232.
19. Caliò I, Pantò B. A macro-element modelling approach of Infilled Frame Structures. *Comput Struct*. 2014;143:91-107. https://doi.org/10.1016/j.compstruc.2014.07.008
20. Pantò B, Caliò I, Lourenço P. Seismic safety evaluation of reinforced concrete masonry infilled frames using macro modelling approach. *Bull Earthq Eng*. 2017;15(9):3871-3895. https://doi.org/10.1007/s10518-017-0120-z
21. Lourenço P. *Computational Strategies for Masonry Structures*. Delft University of Technology; 1997. Doctoral dissertation.
22. Asteris PG, Antoniou ST, Sophianopoulos DS, Chrysostomou CZ. Mathematical macromodeling of infilled frames: state of the art. *J Struct Eng*. 2011;137(12):1508-1517. https://doi.org/10.1061/(asce)st.1943-541x.0000384
23. Smith BS, Carter C. A method of analysis for infilled frames. *Proc Inst Civ Eng*. 1970;46(2):229-231. https://doi.org/10.1680/iicep.1970.6801
24. El-Dakhakhni WW, Elgaaly M, Hamid AA. Three-strut model for concrete masonry-infilled steel frames. *J Struct Eng*. 2003;129(2):177-185. https://doi.org/10.1061/(ASCE)0733-9445(2003)129:2(177)
25. Di Trapani F, Shing PB, Cavaleri L. Macroelement model for in-plane and out-of-plane responses of masonry infills in frame structures. *J Struct Eng*. 2018;144(2):04017198. https://doi.org/10.1061/(asce)st.1943-541x.0001926
26. Caliò I, Marletta M, Pantò B. A new discrete element model for the evaluation of the seismic behaviour of unreinforced masonry buildings. *Eng Struct*. 2012;40:327-338. https://doi.org/10.1016/j.engstruct.2012.02.039
27. 3DMacro-Computer program for the seismic assessment of masonry buildings. *Grup. sismica*, 2009. [Online]. Available: www.grupposismica.it
28. Marques R, Lourenço PB. Unreinforced and confined masonry buildings in seismic regions: validation of macro-element models and cost analysis. *Eng Struct*. 2014;64:52-67. https://doi.org/10.1016/j.engstruct.2014.01.014
29. Pantò B, Rossi PP. A new macromodel for the assessment of the seismic response of infilled RC frames. *Earthq Eng Struct Dyn*. 2019;48(7):792-817. https://doi.org/10.1002/eqe.3163
30. Mazzoni S, McKenna F, Scott MH, Fenves GL. Open System for Earthquake Engineering Simulation (OpenSEES) user command-language manual. *Pacific Earthq Eng Res Cent*. 2006:465.
31. Calvi GM, Bolognini D. Seismic response of reinforced concrete frames infilled with weakly reinforced masonry panels. *J Earthq Eng*. 2001;5(2):153-185. https://doi.org/10.1080/13632460109350390
32. INSYSME INnovative SYStems for earthquake resistant Masonry Enclosures in reinforced concrete buildings. 2016. [Online]. Available: www.insysme.eu
33. Verlato N. *Development of a Clay Masonry Enclosure System With Deformable Joints : Experimental Analysis and Numerical*. Università Degli Studi Di Brescia; 2017. Doctoral dissertation.
34. Smyrou E, Blandon C, Antoniou S, Pinho R, Crisafulli F. Implementation and verification of a masonry panel model for nonlinear dynamic analysis of infilled RC frames. *Bull Earthq Eng*. 2011;9(5):1519-1534. https://doi.org/10.1007/s10518-011-9262-6
35. Kent DC, Park R. Flexural members with confined concrete. *J Struct Div*. 1971;97(7):1969-1990.
36. Dhir PK, Tubaldi E, Ahmadi H, Gough J. Numerical modelling of reinforced concrete frames with masonry infill and rubber joints. *Eng Struct*. 2021;246(July):112833. https://doi.org/10.1016/j.engstruct.2021.112833
37. Tubaldi E, Laura R, Andrea D, Hamid A, Alan M. Measuring bias in structural response caused by ground motion scaling. *Pacific Conf Earthq Eng*. 2017(056):1-6. https://doi.org/10.1002/eqe

38. Noh NM, Liberatore L, Mollaioli F, Tesfamariam S. Modelling of masonry infilled RC frames subjected to cyclic loads: state of the art review and modelling with OpenSees. *Eng Struct*. 2017;150:599-621. https://doi.org/10.1016/j.engstruct.2017.07.002
39. Furtado A, Rodrigues H, Arêde A. Modelling of masonry infill walls participation in the seismic behaviour of RC buildings using OpenSees. *Int J Adv Struct Eng*. 2015;7(2):117-127. https://doi.org/10.1007/s40091-015-0086-5
40. Taylor RL, "FEAP: A Finite Element Analysis Program, Theory Manual. *Manuals*," no. March, 2014.
41. Bolis V, Migliorati L, Stavridis A, Preti M. In-plane behaviour of innovative masonry infills based on different configurations of wooden sliding joints. *Earthq Resist Eng Struct X*. 2015;1:289-301. https://doi.org/10.2495/eres150241

How to cite this article: Dhir PK, Tubaldi E, Pantò B, Caliò I. A macro-model for describing the in-plane seismic response of masonry-infilled frames with sliding/flexible joints. *Earthquake Engng Struct Dyn*. 2022;1-23. https://doi.org/10.1002/eqe.3714